Journal of Natural Fibers

ISSN: (Print) (Online) Journal homepage: https://www.tandfonline.com/loi/wjnf20

Giant Reed (*Arundo donax* L.) Fiber Extraction and Characterization for Its Use in Polymer Composites

Luis Suárez, Mateusz Barczewski, Paulina Kosmela, María D. Marrero & Zaida Ortega

To cite this article: Luis Suárez, Mateusz Barczewski, Paulina Kosmela, María D. Marrero & Zaida Ortega (2022): Giant Reed (*Arundo donax* L.) Fiber Extraction and Characterization for Its Use in Polymer Composites, Journal of Natural Fibers, DOI: 10.1080/15440478.2022.2131687

To link to this article: https://doi.org/10.1080/15440478.2022.2131687

Published online: 15 Oct 2022.

JOURNAL OF NATURAL FIBERS
https://doi.org/10.1080/15440478.2022.2131687

Taylor & Francis
Taylor & Francis Group

Giant Reed (*Arundo donax* L.) Fiber Extraction and Characterization for Its Use in Polymer Composites

Luis Suárez [a], Mateusz Barczewski [b], Paulina Kosmela [c], María D. Marrero [a], and Zaida Ortega [d]

[a]Departamento de Ingeniería Mecánica, Universidad de Las Palmas de Gran Canaria, Las Palmas de Gran Canaria, Spain; [b]Department of Mechanical Engineering, Institute of Materials Technology, Faculty of Mechanical Engineering, Poznan University of Technology, Poznan, Poland; [c]Department of Polymer Technology, Faculty of Chemistry, Gdansk University of Technology, Gdansk, Poland; [d]Departamento de Ingeniería de Procesos, Universidad de Las Palmas de Gran Canaria, Las Palmas de Gran Canaria, Spain

ABSTRACT

This work describes an extraction method for giant reed fibers from stems and leaves based on chemical soaking and crushing through a rolling mill. Obtained fibers, together with the shredded plant (stems + leaves), are characterized in terms of chemical composition, thermal stability, morphology, and crystallinity. Mechanical properties of fibers have also been assessed (single fiber tensile tests). The results show that the proposed method allows obtaining fibers with higher cellulose content (near 70%), good thermal stability (10% weight loss over 270°C), higher density, and better mechanical properties than other *Arundo* fibers previously reported in the literature. Fibers from leaves are thinner and show higher crystallinity than those from stems (72 µm vs. 157 µm, 73% vs. 67% crystallinity, respectively), although mechanical properties are similar for both (around 900 MPa for tensile strength and over 45 GPa for elastic modulus). Analysis of the microstructure shows that fibers consist of microfiber bundles, and the removal of a thin layer of non-cellulosic nature is clear; fibers provide a rougher, cleaner surface than shredded raw material.

摘要

本工作描述了一种从茎和叶中提取巨型芦苇纤维的方法, 该方法基于化学浸泡和通过轧机破碎. 获得的纤维以及切碎的植物 (茎+叶) 具有化学成分、热稳定性、形态和结晶度的特征. 还评估了纤维的机械性能 (单纤维拉伸试验). 结果表明, 与文献中先前报道的其他Arundo纤维相比, 所提出的方法可以获得纤维素含量更高 (接近70%) 、热稳定性好 (270°C以上失重10%) 、密度更高和机械性能更好的纤维. 叶纤维比茎纤维更薄, 结晶度更高 (分别为72 µm和157 µm, 73%和67%结晶度) , 但两者的机械性能相似 (拉伸强度约为900 MPa, 弹性模量超过45 GPa) . 微观结构分析表明, 纤维由超细纤维束组成, 并清除了一层薄薄的非纤维素性质; 纤维提供了比粉碎原料更粗糙、更清洁的表面.

KEYWORDS
Giant reed; *Arundo donax*; natural fibers; characterization

关键词
巨大的芦苇; *Arundo donax*; 天然纤维; 刻画

Introduction

Arundo donax L. is a perennial grass from the *Gramineae* family, with an uncertain origin due to its small size and the high number of chromosomes found in this species, although many authors place it in East Asia (Jensen et al. 2018). Although giant reed produces flowers, seeds are not usually viable, and reproduction takes place through the rhizome or shoot fragmentations. Stems are hollow and have diameters around 2–3 cm, reaching up to 6 m in height, with stem-clasping leaves along the entire stem

CONTACT Luis Suárez luis.suarez@ulpgc.es Edificio de Fabricación Integrada, Parque Científico – Tecnológico de la ULPGC Campus universitario de Tafira Baja, 35017, Las Palmas de Gran Canaria, Las Palmas, Spain

(Csurhes 2016). Giant reed is generally recognized as an interesting source of biomass due to its high productivity and low requirements (Jensen et al. 2018), as it can be grown in almost any type of soil and with a minimal amount of water (Ahmed 2016), with high thermal and pathogen resistance (Accardi et al. 2015).

This species is mainly studied as a feedstock for biorefineries, especially for ethanol and bioenergy products (Accardi et al. 2015; Jensen et al. 2018). Reed has also gained attention for obtaining other biomolecules, such as furfural or levulinic acid, among others (Antonetti et al. 2015; Di Fidio et al. 2020; Raspolli Galletti et al. 2013). Other uses of *Arundo* have been investigated, such as paper and pulp (Shatalov and Pereira 2013), biochar production (Ahmed 2016), as filler in concrete (Ismail and Jaeel 2014), or for oil spill recovery (Piperopoulos et al. 2021). Its cultivation is also proposed as a strategy for soil bioremediation (Fernando et al. 2016; Tarek et al. 2015).

Compared to the extensive research performed on biofuels and biomolecules, only a little attention has been paid to the obtaining of reed composites, mainly related to particle board production (Ferrandez-Garcia et al. 2019; Ferrández Villena et al. 2020; Ferrández-García et al. 2012, 2020; Francesco et al. 2019; García-Ortuño et al. 2011; C. E. Javier et al. 2013; M. T). Those studies on composite production use shredded vegetal material (Bessa et al. 2020, 2021; Fiore et al. 2014; Fiore, Scalici, and Valenza 2014) or bast fibers obtained by combining with a teeth brush (Fiore, Scalici, and Valenza 2014; Scalici, Fiore, and Valenza 2016) or rudimentary mechanical procedures (Ortega et al. 2021; Suárez et al. 2021). From the limited papers found in the literature in this field, these mainly focus on thermoset resins (Bessa et al. 2021; Chikouche et al. 2015; Fiore, Scalici, and Valenza 2014), being polylactic acid (PLA) (Fiore et al. 2014) and polyethylene (PE) used as thermoplastic matrixes (Ortega et al. 2021; Suárez et al. 2021). This paper focuses on the characterization of *Arundo* fibers, obtained from the stems and the leaves, using a combination of chemical and mechanical procedures that provide finer fibers.

Arundo is still considered one of the worst invasive plants in the world (Jiménez-Ruiz et al. 2021), and several actions take place periodically to try to control their spread in many parts of the world. This invasive character is due to its rapid and easy propagation but also to the difficulties in removing its rhizomatous root system. To achieve successful eradication, the continuous application of herbicides, such as glyphosate (Jiménez Auzmendi 2014; Martín, Carolina, and Barroso 2019), or biological/mechanical treatments (Jiménez-Ruiz et al. 2021) are needed, not even arriving to a complete eradication of the plant (Jensen et al. 2018). For example, control campaigns have been performed in Murcia (Aymerich et al. 2012) or Canary Islands (Jiménez Auzmendi 2014) in Spain, Oregon in USA (Martín, Carolina, and Barroso 2019), and Queensland in Australia (Csurhes 2016).

Consequently, a large amount of residual biomass is available in different areas with potential interest as reinforcement of composites, among other possible uses, to advance toward more efficient use of resources and a zero waste strategy.

Materials and methods

Materials preparation

Specimens of *Arundo donax* L. plants have been collected in Gran Canaria (28.081344–15.473501) and show 2–3 cm diameter and around 4–5 m height. The rhizomes were removed, and three different materials were prepared: leaves, stems, and raw material. Leaves and stems were used separately for fiber obtaining. For characterization purposes, all samples were milled in a Retsch ZM 200 mill to a particle size lower than 0.5 mm. All reagents were purchased in analytical grade from Sigma Aldrich and were used without further modification.

Fiber obtaining

Fibers from the stems were obtained after 7–10 days of soaking them in a 1 N NaOH solution and subsequent crushing of the resulting material in a lab-made mechanical device, as described in Suárez

et al. (2021). Once obtained, fibers were washed in water until neutral pH and dried under room conditions for 3–4 days. Fibers were then cut to 3–5 mm length, washed again to remove fine dust, dried at 60°C in a forced air dryer device TG 200 from Retsch, and then sieved in an AS200 Control device from Retsch, using 75 and 800 μm sieves to remove fines and clustered particles.

Fibers from the leaves were also obtained after immersing the green leaves in a 1 N NaOH solution for 3 weeks, and then just by shaking them in water. Once washed, they were cut, washed again, dried, and sieved, as explained for fibers obtained from stems.

Finally, the raw material was chopped, dried at room conditions, and then processed twice in an SM 300 cutting mill from Retsch, using a 10 mm screen. The last step to prepare the shredded material was washing with water, drying with forced air and sieving.

For stems, a fiber extraction yield of around 34% is obtained (on a dry basis), while it is quite lower for leaves (8%). Figure 1 shows the aspect of the obtained materials; fibers are thinner than those obtained in other published works (Fiore, Scalici, and Valenza 2014; Ortega et al. 2021; Suárez et al. 2021).

Chemical characterization

Humidity, ash content, extractives, cellulose, hemicellulose, and lignin were determined. The lignin content was determined using the Klason method according to the ANSI/ASTM 1997a standard (American National Standard Institute 1977), which consists of hydrolysis with H_2SO_4. Acid-soluble lignin (ASL) was determined from the resulting liquor, measuring absorbance at 205 nm, using an extinction coefficient of 110 l/g·cm (Proietti et al. 2017) in a Cary 60 UV–VIS spectrophotometer from Agilent Technologies. Holocellulose content was also determined following a gravimetric method (Browning 1967), in which acetic acid and sodium chlorite were used for the sample delignification. Once this sample was obtained, the total cellulose content was obtained following ANSI/ASTM 1977b standard (American National Standard Institute 1977). Hemicellulose is calculated as holocellulose minus cellulose contents.

Extractive content was determined following NREL/TP-510-42619 (Sluiter et al. 2008), consisting of two subsequent extraction processes, with water and ethanol, respectively.

Three replicas from three different batches were used for all these tests. The results are expressed as average values ± standard deviations.

Density determination

The real density of the samples was measured in an Ultrapyc 5000 Foam gas pycnometer from Anton Paar, using nitrogen as flow gas, at a target pressure of 68.9 kPa (10.0 psi), with temperature control targeted at 20.0°C. A small cell (10 cm^3) was used, running 15 scans per sample under the flow mode and setting the apparatus for fine powder.

Figure 1. Pictures of materials obtained (from left to right): (a) fibers from stems, (b) fibers from leaves, and (c) shredded material.

Fourier Transformed Infrared (FTIR) spectroscopy

FTIR spectra were obtained in a Perkin Elmer spectrum Two spectrophotometer from Perkin Elmer, under the attenuated total reflectance (ATR) mode, from 4000 to 500 cm^{-1}, at a resolution of 4 cm^{-1}, obtaining each spectrum as the average of 64 scans. Intensities in absorbance of peaks at 2900 cm^{-1}, 1420 cm^{-1}, 1375 cm^{-1}, and 893 cm^{-1} have been calculated in Perkin Elmer software to calculate the crystallinity of the samples.

Thermal characterization

Thermogravimetric tests (TGA) were conducted to determine the thermal stability of the samples. TGA was performed in a Netzsch TG 2091F1 Libra apparatus, from 20°C to 900°C at a heating rate of 10°C/min under a nitrogen atmosphere (20 ml/min), using alumina crucibles. The first derivative (DTG) curve was calculated, and values of temperature for 5%, 10%, 20%, and 50% mass loss were determined.

Morphology

Sample dimensions were obtained from optical microscopy observations performed in an Olympus B×51 microscope at 5x and reflected light. A minimum of 50 particles were measured for each sample, with at least 3 measurements per particle.

The sample's morphology was assessed using a Hitachi TM3030 Scanning Electron Microscopy (SEM). Samples were placed in copper tape and coated via electrical glow discharge of Au/Pd target in an SC7620 Mini Sputter Coater from Quorum Technologies. "Fibers" surface and section were observed at different magnifications, at 15 kV.

X-ray diffraction (XRD)

The crystallinity of the samples was obtained from diffraction patterns with Cu Kα radiation (l = 1.5406 Å) in a Seifert URD6 apparatus, using 30 kV and 40 mA. Diffractograms were recorded from $2\theta = 10°$ to $2\theta = 40°$ in 0.05 steps. The presented data were smoothed using the Savitzky–Golay function (polynomial order 2, points of window 15). Crystallinity was determined according to the following equation (Wang et al. 2016):

$$Crystallinity = \frac{(I_{002} - I_{am})}{I_{002}} x100\% \quad (1)$$

where I_{002} is the diffraction intensity of the cellulose I crystalline region (maximum intensity in the 2θ angle range between 20° and 23°), and I_{am} is the diffraction intensity of the amorphous cellulose region (minimum intensity in the 2θ angle range between 18° and 19°).

Mechanical properties

Single fiber tests were performed on leaves and stem fibers to determine their tensile strength and elastic modulus. Thirty fibers were tested per sample in a Dongguan Liyi Test Equipment LY-1065 tester at 1 mm/min rate and a gauge length of 30 mm, following ASTM D3379–75. "Fibers" diameter was determined as the average value of 8 measurements, performed in a micrometer, considering a circular section of the fibers.

Results and discussion

Chemical characterization

Table 1 shows the average values for the obtained fibers and shredded material composition. The composition of the shredded material is similar to *Arundo* stems found in other studies. In particular, ashes have been found in higher content in leaves than in stems (Jensen et al. 2018; Martínez-Sanz et al. 2018), as also found for fibers obtained in this study, being the average content of ashes in stems between 1.9% and 5.5% in most studies (Chikouche et al. 2015; Davide et al. 2016; Shatalov and Pereira 2005). As expected, lignin content for raw shredded material is much higher than for processed fibers, accounting for around 35%; other authors have reported similar values for total lignin, approximately 30% (Davide et al. 2016) and Klason lignin, about 20% for the stems without leaves (Bessa et al. 2021; Suárez et al. 2021).

Total extractives for these materials are below 3.0% due to the fiber extraction or the washing of the shredded material (data not shown). As expected, the process followed for fiber obtaining removes hemicellulose in the plant and leads to a fiber with relatively high cellulose content, in the range of jute or sisal fibers, and, in any case, higher than for fibers obtained in previous works (around 45% (Fiore, Scalici, and Valenza 2014; Suárez et al. 2021)). Lignin content is higher in fibers from stems than in fibers from leaves and within the ranges found in the literature. As stems show a woody rigid structure and contain a higher amount of lignin than leaves, fibers from stems also show higher lignin content than fibers from the leaves. No significant differences in cellulose and hemicellulose content are found for both types of fibers.

Density determination

Table 1 shows the density values for the three materials studied; fibers from leaves show higher density than fibers from stems, which is also higher than from shredded material. For the same species, density measurements can be correlated to the plant's chemical composition (Charca, Tenazoa, and Junior 2021); the material with higher density has higher cellulose content and lower lignin amount. It then appears that *Arundo* fibers obtained in this research show higher density than shredded material and higher cellulose content, as seen in Table 1, due to the procedure followed for fiber extraction. Removing hemicellulose and lignin allows for a higher proportion of cellulose, resulting in a higher density of the fibers. Fiore, Scalici, and Valenza (2014) determined a density for *Arundo* fibers obtained by the mechanical procedure of 1.168 g/cm^3 and cellulose content of 43.59%; fibers obtained here show around 50% more cellulose and densities around 40% higher, while shredded material shows similar composition and density than fibers obtained in that research.

FTIR spectroscopy

Figure 2 shows the average recorded spectra for the samples of shredded material, fibers from leaves, and fibers from stems. Typical bands for lignocellulosic materials can be observed, namely:

- Broad band at 3000–3700 cm^{-1}, assigned to O-H stretching.

Table 1. Composition (in %) and density of shredded material and fiber samples (average values ± standard deviation).

			Lignin				
	Cellulose	Hemicellulose	Klason	ASL	Total	Ashes	Real density (g/cm^3)
Shredded material	38.0 ± 3.7	42.4 ± 1.3	24.9 ± 0.3	8.2 ± 1.0	32.4 ± 2.7	4.9 ± 1.1	1.1727 ± 0.0882
Fibers from stems	67.5 ± 1.9	15.3 ± 4.6	20.4 ± 1.5	5.3 ± 0.1	25.7 ± 0.6	0.4 ± 0.2	1.5456 ± 0.0506
Fibers from leaves	68.8 ± 4.3	20.0 ± 3.8	10.5 ± 2.0	0.8 ± 0.1	11.2 ± 2.2	1.8 ± 0.5	1.6290 ± 0.0538

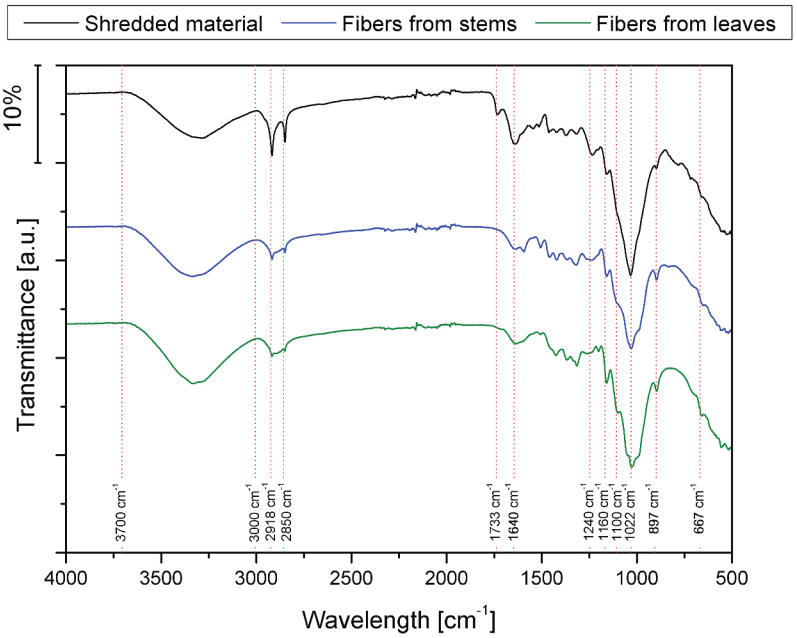

Figure 2. FTIR spectrum for different samples.

- The double peak at 2918 and 2850 cm^{-1}, attributed mainly C-H aliphatic groups in hemicellulose (Chikouche et al. 2015), which decreases in intensity due to the fiber extraction process, is also confirmed in chemical composition assays.
- The sharp peak at 1733 cm^{-1}, related to C=O stretching in lignin and hemicellulose (Bessa et al. 2020; Scalici, Fiore, and Valenza 2016), is found for shredded material but not for fibers. This is correlated with the intensity reduction at 1240 cm^{-1}, also found for fibers, attributed to C-O stretching in lignin (Fiore, Scalici, and Valenza 2014).
- The peak at 1640 cm^{-1} is reduced for fibers, as the removal of hemicellulose and lignin leads to less absorbed water (Martínez-Sanz et al. 2018).
- High-intensity peaks at 1022 cm^{-1} (C=O stretching ring vibration in cellulose) are observed for the three samples, although the relative intensity is higher for fibers than for raw material. This may suggest higher cellulose content for fibers, as observed in the quantification analysis. C-O-C asymmetric stretching at 1160 cm^{-1} also appears clearly for fibers, while it is only a light shoulder for shredded material. The precise definition of a peak at 1100 cm^{-1} may also indicate the higher presence of cellulose I crystals (Martínez-Sanz et al. 2018).

Therefore, in summary, it appears that the procedure proposed for *Arundo* fiber extraction allows obtaining a fiber of good quality to be used in composites, according to the literature, where several treatments (soda, plasma, silanization, etc.) are applied to materials from *Arundo* to improve their surface, in terms of chemical bonding. Fibers obtained only by crushing or peeling show the peak at 1740 cm^{-1}, which can be removed by performing an alkaline treatment (Suárez et al. 2021); this is also in agreement with results obtained from chemical composition tests, which show lower lignin and hemicellulose contents in samples obtained with the procedure described in this paper than for those obtained using only mechanical means.

The Total Crystallinity Index (TCI) and the Lateral Order Index (LOI) can be calculated from FTIR spectra after baseline correction and normalizing (El Oudiani, Msahli, and Sakli 2017), thus giving an approximate idea of the crystallinity of samples. The first one, TCI, is obtained by dividing the absorbance of peaks at 1375 cm^{-1} and 2900 cm^{-1}, being the value obtained proportional to the degree

Table 2. Approximation of crystallinity of samples by FTIR spectrum.

	TCI	LOI	A1620	A897	A667
Shredded material	0.279	0.503	74.817	13.830	4.710
Fibers from stems	0.515	1.026	28.483	18.463	15.140
Fibers from leaves	0.664	0.666	31.560	27.557	13.850

of crystallinity of the cellulose. The second one, LOI, is obtained by dividing absorbance at 1420 cm^{-1} by that at 893 cm^{-1}, considering this last an empirical crystallinity index and also attributed to the proportion of cellulose I (Sang Youn et al. 2005). As observed in Table 2, TCI and LOI values are higher for fiber samples than for shredded materials, thus indicating that fibers show higher crystallinity, a fact that was otherwise expected, as seen in the chemical composition of the three materials. Apparently, fibers from leaves have a higher amount of crystalline cellulose, while fibers from stems have a higher-order degree in the entire structure. Similar conclusions arise if areas of the bands at 1640, 897, and 667 cm^{-1} are considered (Abidi and Manike 2018). A higher area at 1640 cm^{-1} is related to higher water absorption, directly related to higher amorphous content, while more significant areas in the other two peaks are linked to higher cellulose crystallinity.

Thermal characterization

TGA curves for all considered materials show a similar course (Figure 3). However, leaf fibers seem to have higher degradation temperatures than fibers from stems, which are also more stable than shredded material. Residual biomass also has similar values for the three materials.

The most important peak found in the derivative curves is related to cellulose degradation, arising between 338°C and 350°C for these samples (pure cellulose has a maximum pyrolysis rate at 355°C (Yang et al. 2007)); fibers show a higher degradation rate at this peak than shredded material (Table 3). Besides, DTG curves also show some differences in their shape. Only for shredded material samples, the main peak has a shoulder at around 290.8°C due to the hemicellulose degradation (hemicellulose

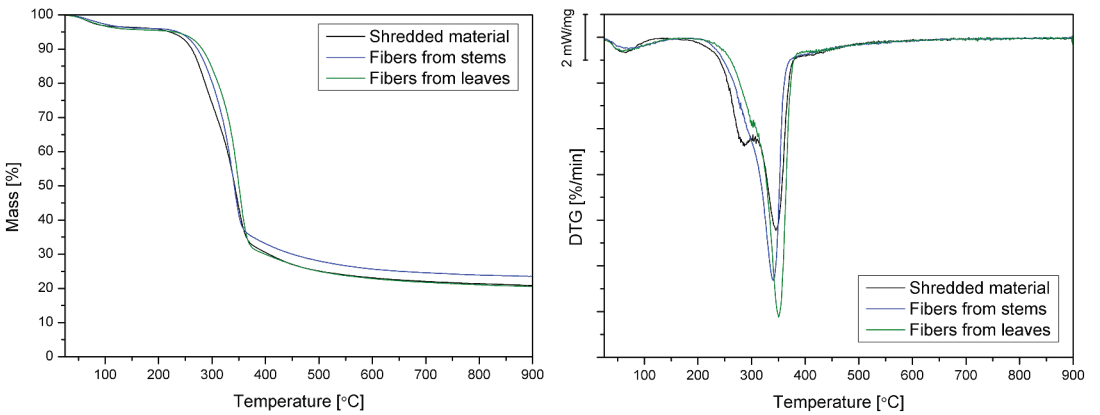

Figure 3. TGA (left) and DTG (right) for stem and leaves fibers and shredded plant.

Table 3. Temperatures for 5%, 10%, 20%, and 50% weight loss, residual mass DTG peak values.

						DTG peak		
	T_5 (°C)	T_{10} (°C)	T_{20} (°C)	T_{50} (°C)	Residual mass (%)	T (°C)	Degradation rate (%/min)	T_d (°C)
Shredded material	226.9	263.9	289.2	343.2	21.64	343.4	7.93	212
Fibers from stems	237.8	273.1	301.3	341.7	23.19	338.5	10.00	233
Fibers from leaves	175.9	280.3	311.0	350.6	20.58	349.9	11.24	237

pyrolysis takes place before cellulose degradation, starting at about 220°C (Bessa et al. 2020)) (Table 3). When considering hemicellulose and cellulose pyrolysis ranges (210–315°C and 315–400°C, respectively), shredded material shows a weight loss of 27.9% in the first step and 37.1% in the second one, being the first decrease considerably lower for fiber samples (23.1% and 16.8% for stems and leaves fibers, respectively), while the α-cellulose-related step shows higher values (39.6% and 48.5%). These values are in the range of those found by other authors for *Arundo*-treated fibers, although with lower peak temperatures (up to 340°C as the maximum value) (Bessa et al. 2020). Scalici and collaborators also obtained the first shoulder on the DTG curve at 285°C and maximum weight loss (30%) at around 340 °C for fibers obtained from leaves (Scalici, Fiore, and Valenza 2016).

Arundo materials obtained and characterized in this work show similar or even higher temperature stability than other fibers from the same species (due to the proposed extraction process) or other vegetal fibers. The onset degradation temperature is found to be around 300°C, thus confirming that it can be considered an excellent candidate to be used in composite production; weight loss starts over 270°C, in the range (or even higher) than other commonly used vegetal fibers, such as flax or jute (Fiore, Scalici, and Valenza 2014). Considering the analyzed fibers as potential reinforcement of thermoplastic composites, it is essential to define the temperature range that will allow their melt processing with polymer without degradation of the lignocellulosic structure. According to the methodology described by Bledzki et al. (Bledzki, Mamun, and Volk 2010), the starting decomposition temperature (T_d) of natural fibers is assumed to be the temperature value associated with a 1% mass loss above 150°C. This approach is due to completely removing free and bonded moisture contents in lignocellulosic fibers below the selected temperature. T_d values are additionally presented in Table 3. The reported test results agree with the spectroscopic analysis results, namely the estimated water absorption determined as the increase in absorbance intensity at 1620 cm^{-1}.

Morphology

Optical microscopy has been used to determine diameters' distribution for the three different samples; fibers obtained from the leaves are thinner (71.6 ± 35.1 μm) than those obtained from the stems (156.5 ± 73.5 μm). Shredded particles show the biggest size (370.3 ± 133.0 μm). As observed in Figure 4, the shredded sample shows some thin fibers (lower than 50 μm in diameter), which were released during the mechanical shredding procedure, although these are merely testimonials. Most fibers have diameters between 50 and 150 microns, while the leaf fibers show an important percentage of fibers under 50 microns and stem fibers between 150 and 250 microns. Shredded material has a uniform distribution at bigger particle sizes (250–350 μm).

On the other hand, SEM micrographs (Figure 5) show clear differences between shredded and fiber samples. Fiber bundles of aligned microfibrils can be observed for all samples, usually happening for cellulosic fibers. These bundles are covered with a layer probably made of lignin or hemicellulose for shredded material (Khan et al. 2020). In contrast, this layer is reduced and appears broken for fiber samples (both from leaves and stems), giving a rougher aspect. This is in agreement with assays performed, which show lower hemicellulose content for fibers than for shredded material. Thinner fibers can be observed for fibers from leaves, as also determined in optical microscopy; this may be due to the higher lignin content, which bonds fibers together, as observed in SEM pictures. Fiber cell wall (Figure S1.c) has the same geometrical structure and different sizes of wall and lumen as already mentioned (Fiore, Scalici, and Valenza 2014). Cellulose is arranged in a spiral shape through the cellular wall; in some samples, elongated vascular cells and pit membranes (Lian et al. 2019) for water and nutrient exchange can also be observed (see Figure S1).

X-ray diffraction (XRD)

The XRD plots presenting X-ray diffraction patterns made for three types of fibers are shown in Figure 6. For all curves, a dominant peak at 2θ in the range of 22–23° can be noted, referred to as the

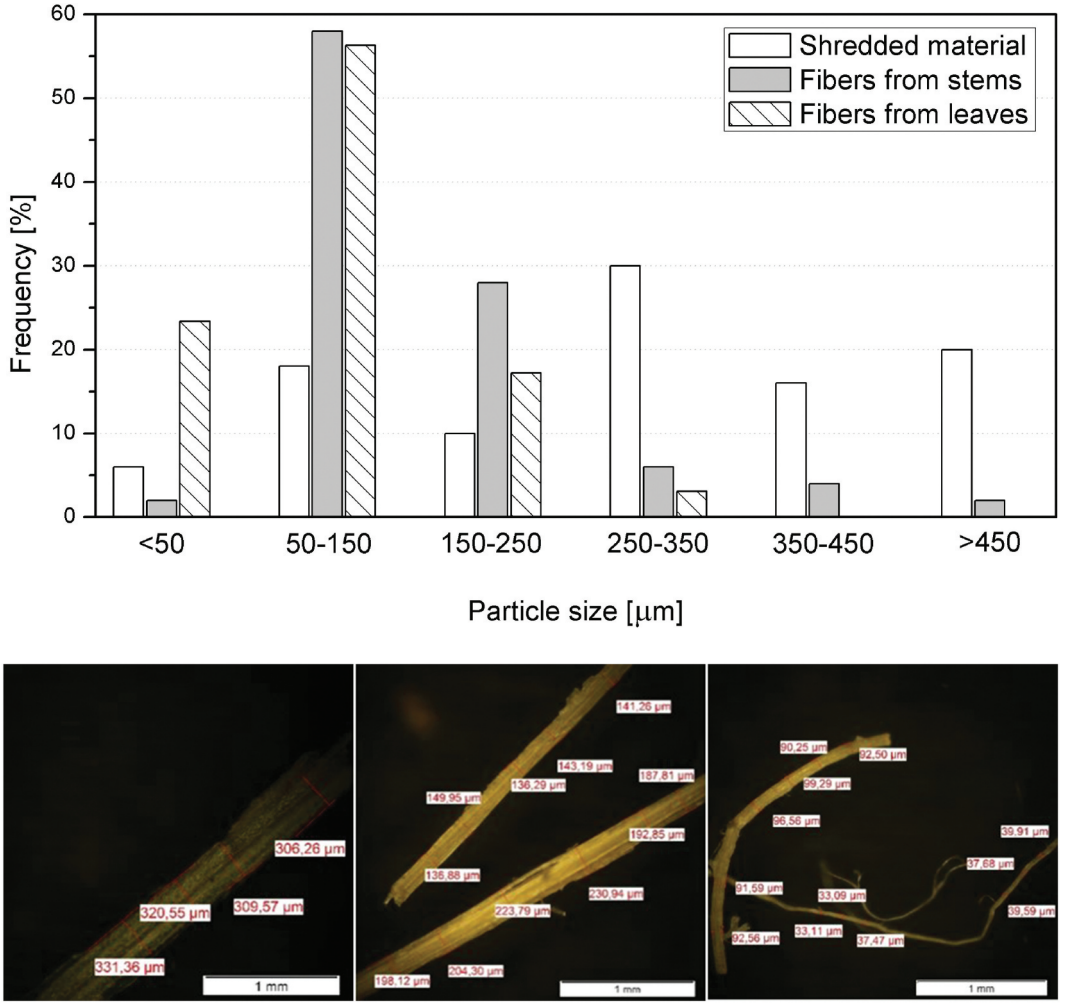

Figure 4. Particle size distribution (frequency vs. particle size, in microns) (above). Pictures from optical microscope and measurements for (a) shredded material, (b) stem fiber, and (c) leaves fiber (below).

crystallographic plane (002) characteristic for crystalline forms of cellulose I (Wang et al. 2016). The curves differ in peak intensities, taking the higher values for fibers and the lowest for shredded material. Additionally, the peak in the (101) crystallographic plane, also attributed to the crystalline cellulose phase (Barreto et al. 2010), is more distinct for fibers from stems. In the result of the calculations made for X-ray data according to Equation (1), the samples of natural fibers showed degrees of crystallinity at the level of 59.1%, 66.7%, and 73.1% for shredded material, fibers from stems, and leaves, respectively. Despite the changeable values concerning TCI resulting from a different methodology (Liu et al. 2012), the trend is comparable; the highest crystallinity characterizes fibers obtained from leaves.

Generally, the higher the cellulose content, the higher the CI. Some authors have even reported a linear correlation between these two parameters (Abidi and Manike 2018). The cellulose in the fibers obtained in this work account for over 65% of the total biomass, and CI is over 60%, while other authors report cellulose contents of 35% and 43% have revealed CI of 50% and 66%, respectively (Bessa et al. 2020; Chikouche et al. 2015). Alkali-treated fibers show higher crystallinity values, increasing up to 58.2% and 75.4%.

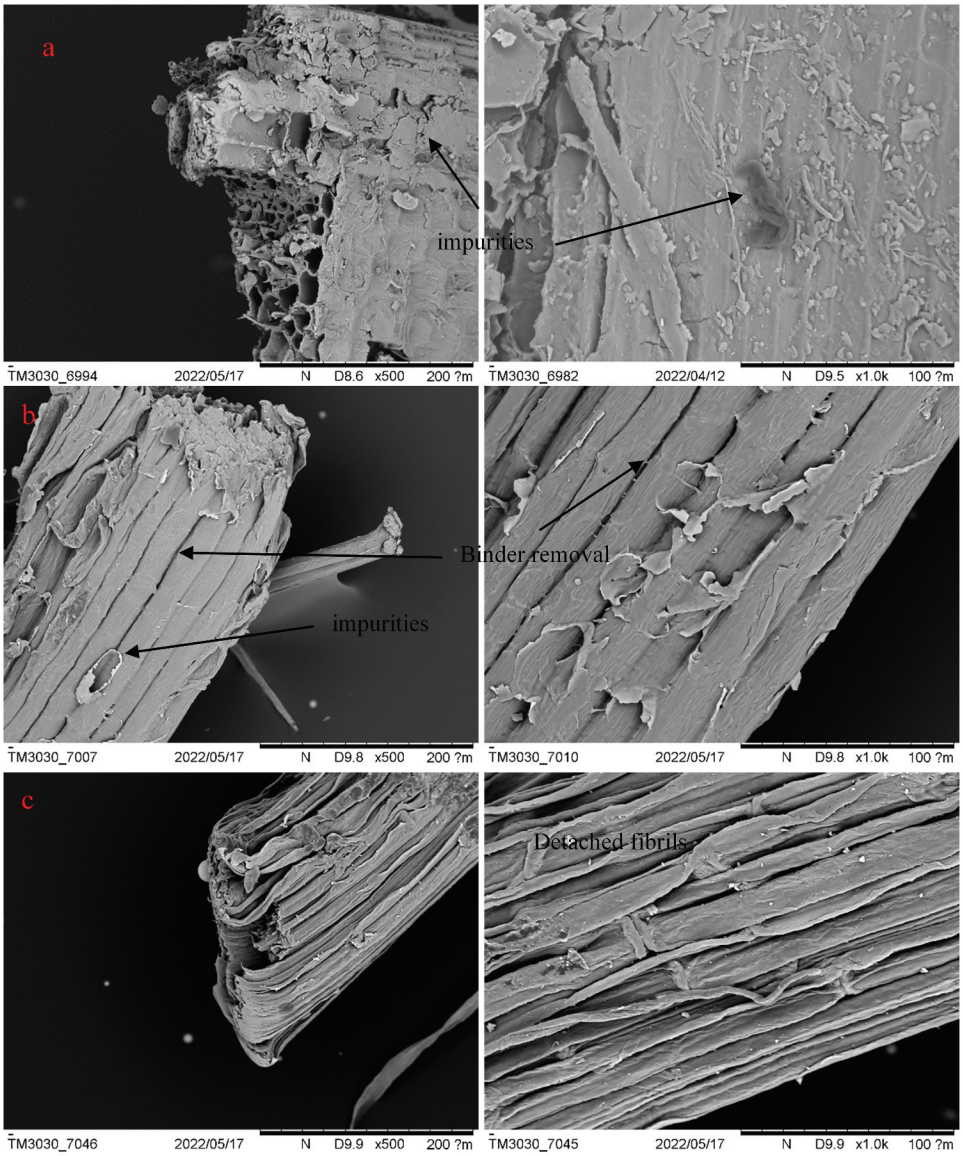

Figure 5. SEM pictures for (a) shredded material, (b) stem fiber, and (c) leaves fiber, at 500x and 1000 x magnifications.

Mechanical properties

Single fiber tests have allowed obtaining tensile strength and elastic modulus for the two types of fibers obtained in this work; fibers from stems show an average strength of around 905 MPa, varying from 600 to 1200 MPa, and an elastic modulus close to 42 GPa (31–56 GPa). Fiore and collaborators (Fiore, Scalici, and Valenza 2014) reported 248 MPa and 9.4 GPa for fibers obtained from stems, which are quite lower than those shown here and those reported for other natural fibers, such as abaca (400–980 MPa; 8–20 GPa), jute (393–773 MPa; 27 GPa), flax (345-1035MPa; 28 GPa) or bamboo (140–1000 MPa, 11–89 GPa) (Odesanya et al. 2021).

Fibers from leaves provide similar values, around 1000 MPa for tensile strength and 39 GPa for elastic modulus, although with higher dispersion of results, especially for modules. Tensile strength varied from 400 to 1500 MPa (a standard deviation of 300 MPa), while elastic modulus values from 12

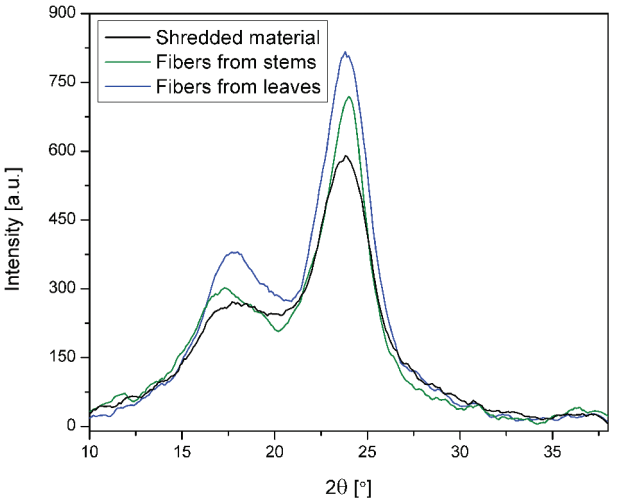

Figure 6. X-ray diffractograms for shredded material, stem fibers, and leaf fibers.

Table 4. Statistical parameters for tensile strength (in MPa) and modulus (in GPa) for *Arundo* fibers.

Tensile strength							
	Average	SD	Median	IQR	Shape parameter	Scale parameter	R^2
Stems	906	323	970	371	2.37	156.92	0.99
Leaves	961	258	962	411	4.10	1058.83	0.97
Modulus							
Stems	42	12	40	13	3.72	46.55	0.97
Leaves	39	19	35	28	1.99	43.89	0.98

to nearly 74 GPa were obtained (19 GPa deviation). This behavior for leaf fibers was also reported in (Scalici, Fiore, and Valenza 2016), although they also received lower values (173.90 ± 146.09 MPa for strength and 15.96 ± 12.17 GPa for modulus). The higher dispersion of results may be related to the increased distribution of diameters found for this material. On the other hand, as observed in SEM pictures, leaf fibers show detached microfibrils, which could explain the variability of results.

Fiber's tensile strength and elastic modulus have been analyzed following a two-parameter Weibull distribution, as found in other works in the literature (Andersons et al. 2005; Fiore, Scalici, and Valenza 2014; Fiore, Valenza, and Di Bella 2011). The probability plots for these two properties can be found in the supplementary material (Figure S2). These graphs show that the data obtained fit a Weibull distribution quite well, as demonstrated by the correlation parameter in Table 4. Table 4 summarizes the statistical parameters obtained in such analysis. For a Weibull distribution, the shape parameter is related to the data variability, while the scale parameter corresponds to the 63.2%ile of the data. In this case, the results obtained are pretty close to normality, as the shape factor is in, or close to, the 2–4 range (Fiore, Valenza, and Di Bella 2011).

Conclusions

This study confirms that *Arundo donax* can be used as a source for high cellulose fibers with interesting mechanical properties and good thermal stability, suitable for thermoplastic composite production. It has been determined that fibers from leaves are thinner (diameter around 70 µm) and show higher crystallinity values (from FTIR and XRD analysis) than fibers from stems, which are thicker (around 150 µm). Thermal stability is similar for both, with an onset temperature of over 300°C. SEM pictures

show the different morphology between shredded material and fibers and not much difference between fibers from stems and leaves, apart from fibrillation and lower fiber diameters. Fibers are formed by microfiber bundles and provide a rough surface due to the removal of binding agents, which may lead to a higher surface and, thus, better attachment to the polymeric matrix.

Highlights

- *Arundo donax* can be used as a source for high cellulose fibers with good mechanical properties
- Leaves fibers are thinner and more crystalline than stem fibers
- *Arundo* fibers show good thermal stability, with an onset temperature of over 300 °C
- The proposed method allows for the obtaining of fibers with good mechanical properties
- Fibers are formed by microfiber bundles and provide a rough surface

Disclosure statement

No potential conflict of interest was reported by the author(s).

Funding

The work was supported by the Agencia Canaria de Investigación, Innovación y Sociedad de la Información [TESIS2021010008].

ORCID

Luis Suárez http://orcid.org/0000-0002-6709-1555
Mateusz Barczewski http://orcid.org/0000-0003-1451-6430
Paulina Kosmela http://orcid.org/0000-0003-4158-2679
María D. Marrero http://orcid.org/0000-0002-9396-1649
Zaida Ortega http://orcid.org/0000-0002-7112-1067

References

Abidi, N., and M. Manike. 2018. X-ray diffraction and FTIR investigations of cellulose deposition during cotton fiber development. *Textile Research Journal* 88 (7):719–30. doi:10.1177/0040517516688634.

Accardi, D. S., P. Russo, R. Lauri, B. Pietrangeli, and L. Di Palma. 2015. From soil remediation to biofuel: Process simulation of bioethanol production from *Arundo donax*. *Chemical Engineering Transactions* 43:2167–72. doi:10.3303/CET1543362.

Ahmed, M. J. 2016. Potential of *Arundo donax* L. stems as renewable precursors for activated carbons and utilization for wastewater treatments: Review. *Journal of the Taiwan Institute of Chemical Engineers* 63 (June):336–43. doi:10.1016/j.jtice.2016.03.030.

American National Standard Institute. 1977. "ANSI/ASTM, 1977b. standard test methods for alpha-cellulose in wood D 1103-60." Washington DC, USA.

Andersons, J., E. Sparniņš, R. Joffe, and L. Wallström. 2005. Strength distribution of elementary flax fibres. *Composites Science and Technology* 65 (3–4):693–702. doi:10.1016/J.COMPSCITECH.2004.10.001.

Antonetti, C., E. Bonari, D. Licursi, N. Nassio Di Nasso, and A. M. Raspolli Galletti. 2015. Hydrothermal conversion of giant reed to furfural and levulinic acid: Optimization of the process under microwave irradiation and investigation of distinctive agronomic parameters. *Molecules* 20 (12):21232–353. doi:10.3390/molecules201219760.

Aymerich, F. R., M. A. E. Selma, I. H. García, V. M. Z. Pérez, P. F. Celdrán, R. V. López, J. M. Fernández, and J. M. Ródenas. 2012. "Seguimiento y Análisis de Las Actuaciones Para El Control Experimental de La Caña Común (Arundo Donax) En La Región de Murcia." Murcia.

Barreto, A. C. H., M. A. Esmeraldo, D. S. Rosa, P. B. A. Fechine, and S. E. Mazzetto. 2010. Cardanol biocomposites reinforced with jute fiber: Microstructure, biodegradability, and mechanical properties. *Polymer Composites* 31 (11):1928–37. doi:10.1002/PC.20990.

Bessa, W., D. Trache, M. Derradji, H. Ambar, M. Benziane, and B. Guedouar. 2021, July. Effect of different chemical treatments and loadings of *Arundo donax* L. fibers on the dynamic mechanical, thermal, and morphological

properties of bisphenol a aniline based polybenzoxazine composites. (pc.26215) *Polymer Composites* 42 (10):5199–208. doi: https://doi.org/10.1002/pc.26215 .

Bessa, W., D. Trache, M. Derradji, H. Ambar, A. F. Tarchoun, M. Benziane, and B. Guedouar. 2020. Characterization of raw and treated *Arundo donax* L. cellulosic fibers and their effect on the curing kinetics of bisphenol a-based benzoxazine. *International Journal of Biological Macromolecules* 164 (December):2931–43. doi:10.1016/j.ijbiomac.2020.08.179.

Bledzki, A. K., A. A. Mamun, and J. Volk. 2010. Barley husk and coconut shell reinforced polypropylene composites: The effect of fibre physical, chemical and surface properties. *Composites Science and Technology* 70 (5):840–46. doi:10.1016/J.COMPSCITECH.2010.01.022.

Browning, B. L. 1967. *Methods of wood chemistry. volumes I & II.methods of wood chemistry. volumes I & II*. New York: Interscience Publishers. Vol. 102. http://www.biblio.com/book/methods-wood-chemistry-volume-1-browning/d/710364055.

Charca, S., C. Tenazoa, and H. S. Junior. 2021. Chemical composition of natural fibers using the measured true density. Case study: Ichu fibers. *Journal of Natural Fibers* 1–6. doi:10.1080/15440478.2021.1952143.

Chikouche, M. D. L., A. Merrouche, A. Azizi, M. Rokbi, and S. Walter. 2015. Influence of alkali treatment on the mechanical properties of new cane fibre/polyester composites. *Journal of Reinforced Plastics and Composites* 34 (16):1329–39. doi:10.1177/0731684415591093.

Csurhes, S. 2016. "Invasive weed risk assessment: Giant reed Arundo Donax." https://www.daf.qld.gov.au/__data/assets/pdf_file/0006/59973/IPA-Giant-Reed-Risk-Assessment.pdf.

Davide, B., A. Salanti, M. Orlandi, D. S. Ali, and L. Zoia. 2016. Biorefinery process for the simultaneous recovery of lignin, hemicelluloses, cellulose nanocrystals and silica from rice husk and *Arundo donax*. *Industrial Crops and Products* 86 (August):31–39. doi:10.1016/j.indcrop.2016.03.029.

Di Fidio, N., A. M. Raspolli Galletti, S. Fulignati, D. Licursi, F. Liuzzi, I. De Bari, and C. Antonetti. 2020. Multi-step exploitation of raw *Arundo donax* L. for the selective synthesis of second-generation sugars by chemical and biological route. *Catalysts* 10 (1):79. doi:10.3390/catal10010079.

Fernando, A. L., B. Barbosa, J. Costa, and E. G. Papazoglou. 2016 January. Giant reed (*Arundo donax* L.). *Bioremediation and Bioeconomy* 77–95. doi:10.1016/B978-0-12-802830-8.00004-6.

Ferrández-García, C. E., J. Andreu-Rodríguez, M. T. Ferrández-García, M. Ferrández-Villena, and T. García-Ortuño. 2012. Panels made from giant reed bonded with non-modified starches. *BioResources* 7 (4):5904–16. doi:10.15376/biores.7.4.5904-5916.

Ferrandez-Garcia, M. T., C. Eugenia Ferrandez-Garcia, T. Garcia-Ortuño, A. Ferrandez-Garcia, and M. Ferrandez-Villena. 2019. Experimental evaluation of a new giant reed (*Arundo donax* L.) composite using citric acid as a natural binder. *Agronomy* 9 (12):882. doi:10.3390/agronomy9120882.

Ferrández-García, M. T., A. Ferrández-García, T. García-Ortuño, C. E. Ferrández-García, and M. Ferrández-Villena. 2020. Assessment of the physical, mechanical and acoustic properties of *Arundo donax* L. biomass in low pressure and temperature particleboards. *Polymers* 12 (6):1361. doi:10.3390/POLYM12061361.

Ferrández Villena, M., C. E. F. Garcia, T. García Ortuño, A. Ferrández García, and M. T. Ferrández García. 2020. The influence of processing and particle size on binderless particleboards made from *Arundo donax* L. rhizome. *Polymers* 12 (3):696. doi:10.3390/polym12030696.

Fiore, V., L. Botta, R. Scaffaro, A. Valenza, and A. Pirrotta. 2014. PLA based biocomposites reinforced with *Arundo donax* fillers. *Composites Science and Technology* 105 (December):110–17. doi:10.1016/j.compscitech.2014.10.005.

Fiore, V., T. Scalici, and A. Valenza. 2014. Characterization of a new natural fiber from *Arundo donax* L. as potential reinforcement of polymer composites. *Carbohydrate Polymers* 106 (1):77–83. doi:10.1016/j.carbpol.2014.02.016.

Fiore, V., A. Valenza, and G. Di Bella. 2011. Artichoke (*Cynara cardunculus* L.) fibres as potential reinforcement of composite structures. *Composites Science and Technology* 71 (8):1138–44. doi:10.1016/J.COMPSCITECH.2011.04.003.

Francesco, B., A. M. Gabarron, J. A. F. Yepes, and J. J. P. Pérez. 2019. Innovative use of giant reed and cork residues for panels of buildings in Mediterranean area. *Resources, Conservation and Recycling* 140 (January):259–66. doi:10.1016/j.resconrec.2018.10.005.

Galletti, A. M. R., C. Antonetti, E. Ribechini, M. P. Colombini, N. N. O Di Nasso, and E. Bonari. 2013. From giant reed to levulinic acid and gamma-valerolactone: A high yield catalytic route to valeric biofuels. *Applied Energy* 102 (February):157–62. doi:10.1016/j.apenergy.2012.05.061.

García-Ortuño, T., J. Andréu-Rodríguez, M. T. Ferrández-García, M. Ferrández-Villena, and C. E. Ferrández-García. 2011. Evaluation of the physical and mechanical properties of particleboard made from giant reed (*Arundo donax* L.). *BioResources* 6 (1):477–86. doi:10.15376/biores.6.1.477-486.

Ismail, Z. Z., and A. J. Jaeel. 2014. A novel use of undesirable wild giant reed biomass to replace aggregate in concrete. *Construction and Building Materials* 67 (September):68–73. doi:10.1016/j.conbuildmat.2013.11.064.

Javier, A.-R., E. Medina, M. T. Ferrandez-Garcia, M. Ferrandez-Villena, C. E. Ferrandez-Garcia, C. Paredes, M. A. Bustamante, and J. Moreno-Caselles. 2013. Agricultural and industrial valorization of *Arundo donax* L. *Communications in Soil Science and Plant Analysis* 44 (1–4):598–609. doi:10.1080/00103624.2013.745363.

Jensen, E. F., M. D. Casler, K. Farrar, J. M. Finnan, R. Lord, C. Palmborg, J. Valentine, and I. S. Donnison. 2018. Giant reed: From production to end use. In *Perennial Grasses for Bioenergy and Bioproducts*, ed. E. Alexopoulou, 107–50. London: Academic Press Inc. Elsevier.

Jiménez Auzmendi, E. 2014. Plantas Invasoras, ¿ Batalla Perdida? ¿ O No ? *Investigación, Gestión Y Técnica Forestal, En La Región de La Macaronesia* 135–55. Universidad de La Laguna. Editor: Juan Carlos Santamarta Cerezal. 2014. 978-84-617-3391-0. Madrid: Colegio de Ingenieros de Montes. Accessed at: https://mdc.ulpgc.es/utils/getfile/collection/MDC/id/177834/filename/218410.pdf

Jiménez-Ruiz, J., L. Hardion, J. P. Del Monte, B. Vila, and M. I. Santín-Montanyá. 2021. Monographs on invasive plants in Europe N° 4: *Arundo donax* L. *Botany Letters* 168 (1):131–51. doi:10.1080/23818107.2020.1864470.

Khan, A., R. Vijay, D. L. Singaravelu, M. R. Sanjay, S. Siengchin, F. Verpoort, K. A. Alamry, and A. M. Asiri. 2020. Characterization of natural fibers from *Cortaderia selloana* grass (pampas) as reinforcement material for the production of the composites. *Journal of Natural Fibers*. doi:10.1080/15440478.2019.1709110.

Lian, C., R. Liu, C. Xiufang, S. Zhang, J. Luo, S. Yang, X. Liu, and B. Fei. 2019. Characterization of the pits in parenchyma cells of the moso bamboo [*Phyllostachys edulis* (Carr.) J. Houz.] Culm. *Holzforschung* 73 (7):629–36. doi:10.1515/HF-2018-0236.

Liu, Y., D. Thibodeaux, G. Gamble, P. Bauer, and D. VanDerveer. 2012. Comparative investigation of Fourier transform infrared (FT-IR) spectroscopy and X-ray diffraction (XRD) in the determination of cotton fiber crystallinity. *Applied Spectroscopy* 66 (8):983–86. doi:10.1366/12-06611.

Martín, S., J. A. G. Carolina, and J. Barroso. 2019. Control of volunteer giant reed (*Arundo donax*). *Invasive Plant Science and Management* 12 (1):43–50. doi:10.1017/inp.2018.36.

Martínez-Sanz, M., E. Erboz, C. Fontes, and A. López-Rubio. 2018. Valorization of *Arundo donax* for the production of high performance lignocellulosic films. *Carbohydrate Polymers* 199 (November):276–85. doi:10.1016/j.carbpol.2018.07.029.

Odesanya, K. O., R. Ahmad, M. Jawaid, S. Bingol, G. O. Adebayo, and Y. H. Wong. 2021. Natural fibre-reinforced composite for ballistic applications: A review. *Journal of Polymers and the Environment* 29 (12):3795–812. doi:10.1007/s10924-021-02169-4.

Ortega, Z., F. Romero, R. Paz, L. Suárez, A. N. Benítez, and M. D. Marrero. 2021. Valorization of invasive plants from macaronesia as filler materials in the production of natural fiber composites by rotational molding. *Polymers* 13 (13):2220. doi:10.3390/polym13132220.

Oudiani, A. E., S. Msahli, and F. Sakli. 2017. In-depth study of agave fiber structure using Fourier transform infrared spectroscopy. *Carbohydrate Polymers* 164 (May):242–48. doi:10.1016/J.CARBPOL.2017.01.091.

Piperopoulos, E., A. Khaskhoussi, V. Fiore, and L. Calabrese. 2021. Surface modified *Arundo donax* natural fibers for oil spill recovery. *Journal of Natural Fibers* 1–16. doi:https://doi.org/10.1080/15440478.2021.1961343.

Proietti, S., S. Moscatello, M. Fagnano, N. Fiorentino, A. Impagliazzo, and A. Battistelli. 2017. Chemical composition and yield of rhizome biomass of *Arundo donax* L. grown for biorefinery in the Mediterranean environment. *Biomass & Bioenergy* 107 (December):191–97. doi:10.1016/j.biombioe.2017.10.003.

Sang Youn, O., D. I. Yoo, Y. Shin, H. C. Kim, H. Y. Kim, Y. S. Chung, W. H. Park, and J. H. Youk. 2005. Crystalline structure analysis of cellulose treated with sodium hydroxide and carbon dioxide by means of X-ray diffraction and FTIR spectroscopy. *Carbohydrate Research* 340 (15):2376–91. doi:10.1016/J.CARRES.2005.08.007.

Scalici, T., V. Fiore, and A. Valenza. 2016. Effect of plasma treatment on the properties of *Arundo donax* L. leaf fibres and its bio-based epoxy composites: A preliminary study. *Composites Part B: Engineering* 94 (June):167–75. doi:10.1016/j.compositesb.2016.03.053.

Shatalov, A. A., and H. Pereira. 2005. Kinetics of organosolv delignification of fibre crop *Arundo donax* L. *Industrial Crops and Products* 21 (2):203–10. doi:10.1016/j.indcrop.2004.04.010.

Shatalov, A. A., and H. Pereira. 2013. High-grade sulfur-free cellulose fibers by pre-hydrolysis and ethanol-alkali delignification of giant reed (*Arundo donax* L.) stems. *Industrial Crops and Products* 43 (1):623–30. doi:10.1016/j.indcrop.2012.08.003.

Sluiter, A., R. Ruiz, C. Scarlata, J. Sluiter, and D. And Templeton NREL/TP-510-42619 - Determination of Extractives in Biomass: Laboratory Analytical Procedure (LAP). Technical Report NREL/TP-510-42619. January 2008. Accessible on: https://www.nrel.gov/docs/gen/fy08/42619.pdf

Suárez, L., J. Castellano, F. Romero, M. D. Marrero, A. N. Benítez, and Z. Ortega. 2021. Environmental hazards of giant reed (*Arundo donax* l.) in the Macaronesia region and its characterisation as a potential source for the production of natural fibre composites. *Polymers* 13 (13):2101. doi:10.3390/polym13132101.

Tarek, A., N. Elhawat, É. Domokos-Szabolcsy, J. Kátai, L. Márton, M. Czakó, H. El-Ramady, and M. G. Fári. 2015. Giant reed (*Arundo donax* L.): A green technology for clean environment. *Phytoremediation: Management of Environmental Contaminants* 1:1–20. doi:10.1007/978-3-319-10395-2_1.

Wang, C., S. Bai, X. Yue, B. Long, and L. P. Choo-Smith. 2016. Relationship between chemical composition, crystallinity, orientation and tensile strength of kenaf fiber. *Fibers and Polymers* 2016 (11):1757–64. doi:10.1007/S12221-016-6703-5.

Yang, H., R. Yan, H. Chen, D. H. Lee, and C. Zheng. 2007. Characteristics of hemicellulose, cellulose and lignin pyrolysis. *Fuel* 86 (12–13):1781–88. doi:10.1016/j.fuel.2006.12.013.